IOP Publishing Journal of Physics D: Applied Physics
J. Phys. D: Appl. Phys. **55** (2022) 275202 (14pp) https://doi.org/10.1088/1361-6463/ac5da5

Plasma asymmetry and electron and ion energy distribution function in capacitive discharges excited by tailored waveforms

Sarveshwar Sharma[1,2,*], **Nishant Sirse**[3,*], **Animesh Kuley**[4] and **Miles M Turner**[5]

[1] Basic Theory and Simulation Division, Institute for Plasma Research, Gandhinagar 382428, India
[2] Homi Bhabha National Institute, Anushaktinagar, Mumbai 400094, India
[3] Institute of Science & Research, IPS Academy, Indore 452012, India
[4] Department of Physics, Indian Institute of Science, Bangalore, Karnataka 560012, India
[5] School of Physical Sciences and National Center for Plasma Science and Technology, Dublin City University, Dublin 9, Ireland

E-mail: sarvesh@ipr.res.in and nishantsirse@ipsacademy.org

Received 19 November 2021, revised 1 March 2022
Accepted for publication 14 March 2022
Published 14 April 2022

Abstract

Using a particle-in-cell simulation technique, we investigate the plasma and ionization asymmetry, higher harmonics generation, and electron and ion energy distribution function (IEDF) in capacitive discharges excited by tailored waveforms. At a base frequency of 13.56 MHz, three different waveforms, namely sinusoidal, sawtooth, and square, are applied for a constant current density amplitude of 50 A m^{-2} and gas pressure of 5 mTorr. The simulation results show that the square waveform produces the highest plasma density in the discharge, whereas maximum asymmetry is observed for plasma excited by the sawtooth-like waveform. Both square and sawtooth waveforms generate multiple beams of high-energy electrons from near to the expanding phase of the sheath edge and high-frequency modulations up to 100 MHz on the instantaneous sheath position. The electron energy distribution function depicts three electron temperature and highly elevated tail-end electrons for the square waveform in comparison to the sinusoidal and sawtooth waveform. The IEDF is bimodal at both the powered and grounded electrodes with a large asymmetry and narrow-type distribution in the case of the sawtooth-like waveform. These results suggest that the choice of waveform is highly critical for achieving maximum asymmetry and plasma density simultaneously in capacitive discharges.

Keywords: capacitive discharges, tailored waveform, PIC simulation, plasma asymmetry, higher harmonics, electron and ion energy distribution function

(Some figures may appear in color only in the online journal)

1. Introduction

Low pressure capacitively coupled plasma (CCP) discharges can be operated by either current- or voltage-driven radio-frequency (RF) waveforms applied between a pair of electrodes. In semiconductor industries, CCP is one of the most important plasma-processing tools for the fabrication of large-scale integrated circuits [1]. In order to achieve uniform processing over the substrate, it is crucial to have control on some of the critical plasma sheath parameters like the ion flux and ion energy. Higher ion flux is required for enhancing the processing rate, which depends on the plasma density, whereas lower energy is beneficial for preventing surface

* Authors to whom any correspondence should be addressed.

damage. In CCP discharges operated by single frequency sinusoidal waveforms, higher densities can be achieved either by applying higher voltages or higher frequencies and by keeping all other controlling parameters constant [1–16]. On the other hand, a dual-frequency waveform-operated CCP discharge produces high-density plasmas either by the variation of high-frequency voltage amplitude, or the higher frequency itself also provides an additional control on the ion energy by changing the lower frequency parameters [17–30].

Generation of plasma using non-sinusoidal waveforms is another alternative for achieving control on the plasma sheath parameters and asymmetry in the discharge [31–42]. A popular terminology used for these non-sinusoidal waveforms are 'tailored waveforms', which can be created by the superimposition of fundamental frequency and its higher harmonics with suitable phase shift between them [43–46]. The benefits of tailored waveform-excited CCP discharges were first demonstrated by Patterson *et al* [31] who showed that, by increasing the number of harmonics, the plasma density and ion flux increased significantly. Using hybrid simulation, Heil *et al* [32, 33] showed that a DC self-bias can be generated even in a geometrically symmetrical reactor using a fundamental frequency and its second harmonic, called the electric asymmetry effect. Donko *et al* further demonstrated that, using phase-separated waveforms, the ion flux stays nearly constant, and the self-bias, and hence the maximum ion energy, changes significantly [34]. Further studies performed by increasing the number of harmonics in the tailored waveform have shown that the ion flux and average ion energy on one of the electrodes can be enhanced without changing it on the other electrode [47–50]. This effect was attributed to the ionization asymmetry that produces more intense ionization on one of the electrodes compared to the other electrode. In processing applications, the use of tailored waveforms played an important role in thin film deposition [51, 52] and silicon etching [53, 54].

The use of a temporal asymmetric waveform for generating an asymmetric plasma response was also investigated. In recent years, several simulation and experimental studies have been performed to investigate the CCP discharges excited by temporal asymmetric waveforms, particularly using a sawtooth-like waveform [38–40, 42]. A simulation study performed by Bruneau *et al* [38] used different rise and fall slopes of sawtooth voltage waveforms and demonstrated that a high ionization rate occurs in the vicinity of the sheath edge near to the powered electrode because of the rapid sheath expansion. The ionization spatial asymmetry obtained using such waveforms has been demonstrated experimentally using phase-resolved optical emission spectroscopy [40]. Further studies performed at different gas pressures showed that the flux asymmetry decreases at low gas pressure [39]. Using a 1D3V particle-in-cell (PIC) method, Sharma *et al* [42] demonstrated the influence of driving frequency on plasma density, discharge asymmetry, and electric field nonlinearity for a sawtooth-like current waveform. It was shown that the formation of high-frequency sheath edge oscillations at lower RF driving frequency creates higher plasma density. The burst-like structures in time averaged J.E (i.e. alternate electron heating and cooling) was observed, which suggested that the heating mechanism cannot be described by using a simple analytical model [42]. One of the studies performed by Donko *et al* [55] compared ion energy and angular distribution in CCP excited by single-frequency, classical dual-frequency, valleys, and sawtooth-type waveforms. Their results showed that the valley-type waveform produces controlled narrow ion energy distribution when compared to the classical dual-frequency waveform. On the other hand, a sawtooth-type waveform has shown minimal effect on the angular distributions.

Most of the previous works using tailored waveforms focus on one kind of waveform; however, there exist very few studies comparing different tailored waveforms and their comparison with a sinusoidal waveform. In the present work, we investigate the discharge asymmetry, electron beam generation, and high-frequency sheath modulation along with electron and ion energy distribution function (IEDF) in CCP discharge using two different temporally asymmetric waveforms, namely sawtooth-type and square waveforms, and make comparisons with plasma excited by a sinusoidal waveform at a fundamental RF frequency of 13.56 MHz.

The paper is organized as follows. Details of the simulation parameters and a description of the simulation technique, which is based on a PIC/Monte Carlo collision (PIC/MCC) method, is given in section 2. A physical explanation of the simulation results is described in section 3. A summary and conclusion of the paper is given in section 4.

2. Simulation technique and parameters

A self-consistent 1D3V electrostatic PIC code was used to simulate a symmetrical CCP discharge for the argon plasma. This code is well tested, benchmarked, and comprehensively used in several research papers. A few of the important references can be found here [11–14, 56–62]. The code is based on the PIC/MCC technique and essential features of this method are given in the literature [63, 64]. This code can handle both current- and voltage-driven cases and, for the present study, we used the current-driven mode. The particulars of the simulation procedure adopted in the code are reported in [65]. All the critical particle-particle collision reactions viz. ion-neutral (inelastic, elastic, and charge exchange), electron-neutral (ionization, elastic, and inelastic), and processes like metastable pooling, multi-step ionization, super elastic collisions, partial de-excitation, and further de-excitation are considered here. The different types of reactions included in all sets of simulations are given in [13]. The production of metastables (Ar^* and Ar^{**}) are considered and tracked in the output diagnostics.

In the simulation, we have considered the charge particles like electrons, ions, and the two lumped excited states of Ar (Ar^* ($3p^5 4s$), 11.6 eV, and Ar^{**} ($3p^5 4p$), 13.1 eV) with a neutral argon gas background. The particulars of the species considered in the simulation, the detailed reactions, and the cross-sections are taken from well-tested sources and can be found in the literature [13, 58, 66]. The grid size (Δx) and time step size (Δt) is chosen in such a way that can resolve the Debye length ($\lambda_{De} = \sqrt{\varepsilon_0 k_B T_e / n_e e^2}$) and the electron plasma frequency ($f_{pe} = \sqrt{n_e e^2 / \varepsilon_0 m_e}/2\pi$), respectively,

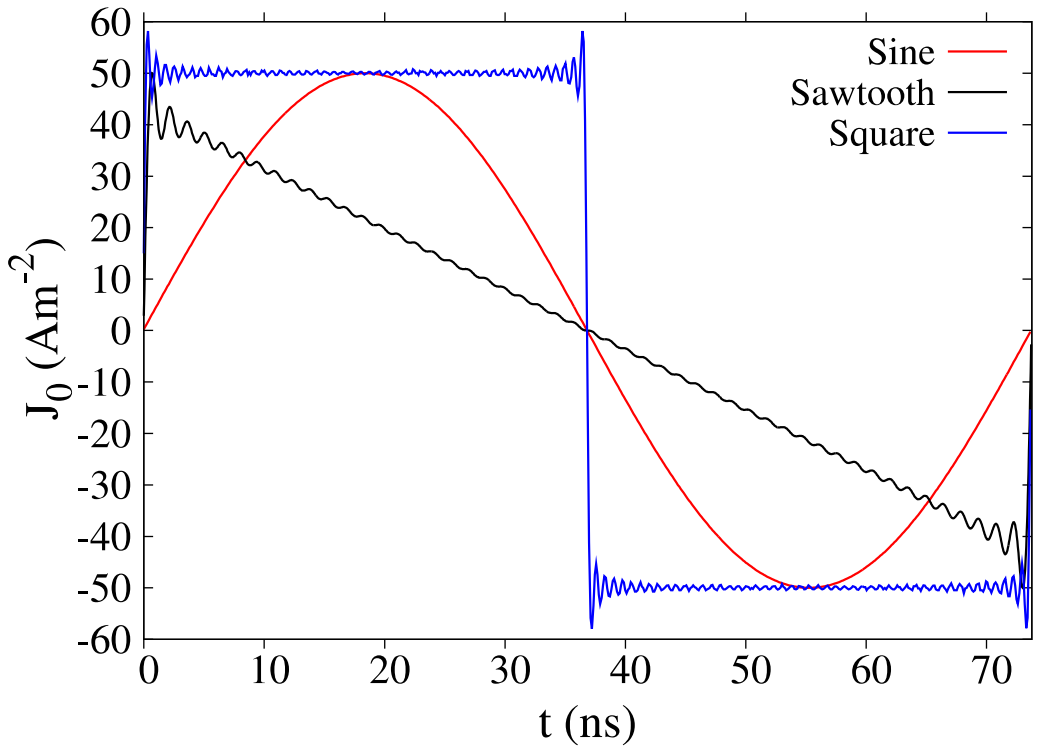

Figure 1. Current profile of sinusoidal, sawtooth, and square waveforms for a base frequency of 13.56 MHz with a current density amplitude of 50 A m^{-2}.

so that the stability and accuracy criterion of the PIC can be found.

The electrodes considered here are planar and parallel to each other, having infinite dimension. The gap between electrodes is 6 cm and the operating neutral gas pressure is 5 mTorr. The electrodes are assumed perfectly absorbing, and the secondary electron emission (SEE) is ignored. This is due to the low-pressure conditions. Mostly, SEE phenomena are dominant in the high-pressure regime. At high pressure, the density is high and the sheath width is narrow compared to the low pressure/density case, so the electric field inside the sheath is very sharp, which provides more acceleration to ions and gains high energy causing SEE from the electrode. Secondary electrons in metals are known to come from a region between 10^{-7} and 10^{-8} cm thick; ions with energies of the order of MeV penetrate to depths of the order of 10^{-8} cm [67]. A recent study [68] showed that the SEE might play a significant role even at low gas pressure depending on the discharge voltage. In the present case, the discharge voltage is below 500 V for the sawtooth waveform. Therefore, SEE will not play a major role here. For the square waveform, the discharge voltage is higher ($\sim$1000 V) and therefore omitting SEE will underestimate the plasma density. Overall, the asymmetry and distribution functions will not change significantly. In the simulation, the neutral argon gas is uniformly distributed, having a fixed temperature of 300 K. The ion temperature is also the same as the neutral gas temperature. The number of particles per cell for all sets of simulations is 100. All the simulations run for more than 5000 RF cycles to achieve a steady state profile.

Three different types of current waveforms, namely sinusoidal, sawtooth, and square, are used here. The complex structures of waveforms like sawtooth and square can be generated by superimposition of a reasonable number of harmonics of a fundamental RF frequency and also by logically picking the phase shifts between them. For current-driven CCP, the following are the mathematical expressions for sinusoidal, sawtooth, and square waveforms (see figure 1):

$$J_{\mathrm{rf}}(t) = J_0 \sin(\omega_{\mathrm{rf}} t) \tag{1}$$

$$J_{\mathrm{rf}}(t) = \pm J_0 \sum_{k=1}^{N} \frac{1}{k} \sin(k\omega_{\mathrm{rf}} t) \tag{2}$$

$$J_{\mathrm{rf}}(t) = J_0 \sum_{k=0}^{N} \frac{\sin[(2k+1)\omega_{\mathrm{rf}} t]}{2k+1} \tag{3}$$

where, in equation (2), the positive and negative signs represent 'sawtooth-down' and 'sawtooth-up' waveforms, respectively. Here, J_o is the amplitude of current density, which is applied at the powered electrode, and ω_{rf} is the fundamental angular driven radio-frequency. The magnitude J_0 varies with the total number of harmonics N (which is 50 here for sawtooth and square waveforms) and is organized in a way to construct the required peak-to-peak current density amplitude. We have used the 'sawtooth-down' current waveform. Figure 1 shows the profile of sinusoidal, sawtooth, and square waveforms for a base frequency of 13.56 MHz with a current density amplitude of 50 A m^{-2}. The choice of current-driven CCP discharge is arbitrary here because the main motivation of the present research work is to investigate the effect of different current waveforms (sinusoidal, sawtooth, and square) on the

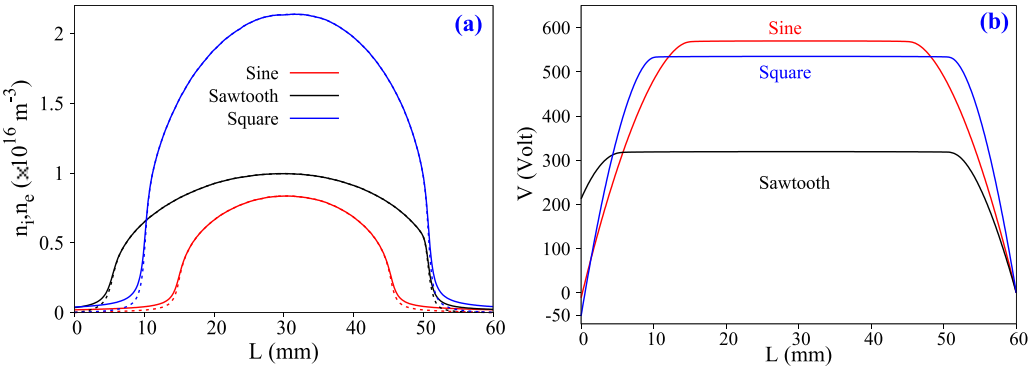

Figure 2. (a) The spatial profile of time-averaged ion (solid line) and electron density (dashed line) and (b) time-averaged potential profiles for different waveforms (sine, sawtooth, and square) at 13.56 MHz applied frequency. The current density amplitude is 50 A m^{-2}.

plasma parameters and sheath dynamics. Moreover, most of the analytical models are based on current-driven cases so direct comparison of the simulation results with them is relatively straightforward [69, 70]. In the experiments, such waveforms are produced by using an arbitrary waveform generator that, upon amplification by using a wideband power amplifier, could be utilized for the plasma generations. A desired waveform with minimum distortion could be obtained by using a feedback-correction loop [31] similar to the one used in the case of arbitrary voltage waveform generation.

3. Results and discussions

For a constant driving frequency, the shape of the applied waveform greatly alters the sheath dynamics and, therefore, the plasma profile eventually modifies. Figure 2(a) presents the spatial profile of time-averaged electron and ion density in the discharge for different current waveforms; i.e. sinusoidal, sawtooth, and square. The fundamental driving frequency is 13.56 MHz, and the current density amplitude is 50 A m^{-2} for all the cases. The argon pressure is kept constant at 5 mTorr for all sets of simulations. In figure 2(a), the current source is applied at $L = 0$ mm and the electrode at 60 mm is grounded. As shown in figure 2(a), the central plasma density is $\sim 8.4 \times 10^{15}$ m^{-3}, $\sim 1 \times 10^{16}$ m^{-3}, and $\sim 2.1 \times 10^{16}$ m^{-3} for the sinusoidal, sawtooth, and square waveform, respectively. Thus, the density formation is highest in the case of the square waveform, which is typically 2.5 times higher compared to the sinusoidal waveform. The corresponding ion flux measured at the grounded electrode is 7.5×10^{18} m^{-2} s^{-1} and 1.7×10^{19} m^{-2} s^{-1} for the sinusoidal and square waveform, respectively, which indicates that the latter is $\sim$2.3 times more compared to the former.

As discussed in section 1, higher plasma density and therefore an enhanced ion flux at the electrode is the fundamental criterion for an improved plasma-processing rate. Therefore, the square waveform is far better for achieving a higher processing rate in comparison to the sinusoidal waveform. In contrast to the higher plasma density observed in the case of the square waveform, the sawtooth waveform presents a larger bulk plasma length. The sheath width at the powered/grounded electrode is 6 mm/9.7 mm and 10.4 mm/9.5 mm for the sawtooth and square waveforms, respectively. For the sinusoidal waveform, the sheath width near to the electrodes is approximately the same ($\sim$15 mm). The sheath width is calculated by observing the maximum position of the electron sheath edge from the electrode and where the quasi-neutrality breaks down.

Regarding plasma asymmetry, it is observed that the sawtooth waveform shows maximum asymmetry. The corresponding DC self-bias (figure 2(b)) is highest for the sawtooth waveform ($\sim$210 V), which represents strong asymmetry, whereas the square waveform generates a minimal negative DC self-bias of $\sim$50 V. On the other hand, the DC self-bias is negligible in the case of the sinusoidal waveform and therefore no discharge asymmetry is present. A plot of time-averaged potential profiles for all the waveforms is displayed in figure 2(b) showing the formation of DC self-bias on the powered electrode. Similar trends, i.e. higher discharge asymmetry and plasma density in the case of the sawtooth and square waveform, respectively, is observed at 100 A m^{-2} current density amplitude. At 100 A m^{-2}, the DC self-bias is zero in the case of the sinusoidal waveform, whereas the sawtooth and square waveform show a DC self-bias of $\sim$470 and -300 V, respectively. On the other hand, the maximum plasma density is $\sim 1.2 \times 10^{16}$ m^{-3}, $\sim 2.5 \times 10^{16}$ m^{-3}, and $\sim 5 \times 10^{16}$ m^{-3} for the sinusoidal, sawtooth, and square waveforms respectively, which is again highest for the square waveform. However, the results are included below due to the higher discharge voltage conditions for achieving higher current density amplitude and thus SEE may be important. This will be subject to future investigation.

An enhancement in the plasma density by changing the shape of the current waveform can be understood by analyzing the ionization rate within the discharge system. Figure 3 shows the time-averaged ionization rates along with the excitation rates at a current density amplitude of 50 A m^{-2} for three different waveforms. For low gas pressure, the electron means the free path is longer and hence the ionization and excitation mechanisms mainly occur inside the bulk plasma. Figure 3(a) shows the direct ionization ($e + Ar \rightarrow 2e + Ar^+$) while the electron collides with the ground state argon atom. It is clear from the figure that the overall direct ionization rate

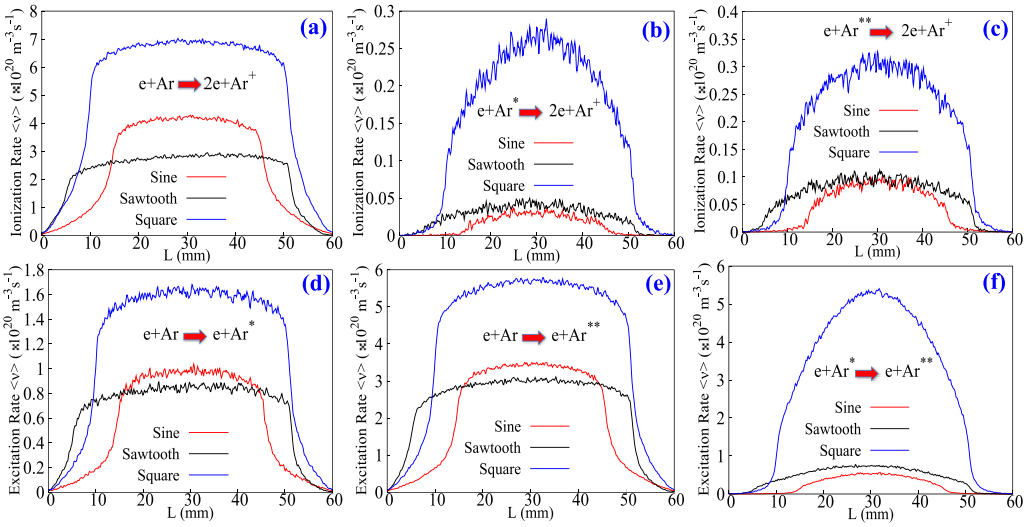

Figure 3. Time-averaged ionization (a)–(c) and excitation (d)–(f) rates at different applied current waveforms (sinusoidal, sawtooth, and square) for 13.56 MHz RF frequency and current densities of 50 A m^{-2}.

is highest for the square waveform. The sinusoidal waveform has a higher ionization rate in the bulk plasma compared to the sawtooth waveform; however, it is drastically lower near to the electrodes; i.e. up to 15 mm from both electrodes. Figures 3(b) and (c) show the multi-step ionization that occurs when electrons impact with metastable state Ar^* ($e + Ar^* \rightarrow e + Ar^+$) and Ar^{**} ($e + Ar^{**} \rightarrow e + Ar^+$), respectively.

Although the contribution from such processes is lower in comparison to the direct ionization (figure 3(a)), we can observe that the multi-step ionization process rate is highest in the case of the square waveform. Comparing the sawtooth with the sinusoidal waveform, we can distinctly observe that the sawtooth waveform has the highest ionization rate for both cases here. These two processes along with the direct ionization are producing higher plasma density in the case of the sawtooth waveform compared to the sinusoidal profile.

Figures 3(d) and (e) show the production of metastable Ar^* ($e + Ar \rightarrow e + Ar^*$) and Ar^{**} ($e + Ar \rightarrow e + Ar^{**}$) from neutral gas. The square waveform has a very high population of Ar^* ($3p^5 4s$, 11.6 eV) and Ar^{**} ($3p^5 4p$, 13.1 eV) in all three cases. Although the central metastable densities (Ar^* and Ar^{**}) are higher for the sinusoidal in comparison to the sawtooth waveform, however the average metastable densities production ($Ar^* = 5.5 \times 10^{19} m^{-3}$ for sine and $6.5 \times 10^{19} m^{-3}$ for sawtooth, $Ar^{**} = 1.9 \times 10^{20} m^{-3}$ for sine and $2.3 \times 10^{20} m^{-3}$ for sawtooth) is higher for the sawtooth waveform. It is also important to notice from figures 3(d)–(f) that the production of Ar^{**} is higher compared to Ar^* in all the cases. The low-energy electrons (~1.5 eV) are further absorbed in excitation from Ar^* to Ar^{**} ($e + Ar^* \rightarrow e + Ar^{**}$) and its production rate is utmost in the square waveform and lowest for the sinusoidal waveform (see figure 3(f)).

The observed asymmetries when the applied waveform is changed are mainly due to an asymmetry in the spatio-temporal ionization dynamics. To elucidate this, we further investigate the ionization mechanism by examining the spatio-temporal profile of the ionizing collision rate for three different current waveforms. This is plotted in figure 4 for two RF periods averaged over the last 600 RF cycles. As shown in figure 4(a), for the sinusoidal waveform, the ionization profile is symmetrical and broad, and the maximum ionizing collision rate is observed during the time of sheath expansion at both the grounded and powered electrodes. Moreover, the ionizing front penetrates the bulk plasma and reaches the opposite sheath because of the nearly collisionless operating conditions. Figure 4(b) shows the spatio-temporal profile of the ionizing collision rate for the sawtooth waveform, which has the highest asymmetry (also see figure 1); i.e. a strong ionization is observed near to the grounded sheath compared to the power electrode sheath. Here, multiple beams of energetic electrons emerge during the expanding phase of the sheath near to the grounded electrode that penetrate the bulk plasma and approach the opposite sheath edge.

The spatio-temporal profile of the ionizing collision rate for the square waveform is displayed in figure 4(c). Here, the profile nearly turns symmetrical, and multiple bursts of high-energy electrons emerge from the expanding phase of the sheath edge. The intensity of these bursts is higher in comparison to the sawtooth and sinusoidal waveforms. Comparing sheath velocities on the grounded electrodes for different waveforms shows it is highest for the square waveform (7.35×10^5 m s^{-1}) and lowest for the sinusoidal waveform (2.2×10^5 m s^{-1}). The sheath velocity for the sawtooth waveform is 4.97×10^5 m s^{-1}. The higher sheath velocity enhances the energy gained by the oscillating electrons and henceforth the ionizing collision rate, and therefore the plasma density, also goes up. Further, by looking at the figure of the spatio-temporal ionizing collision rate, it is clearly observed

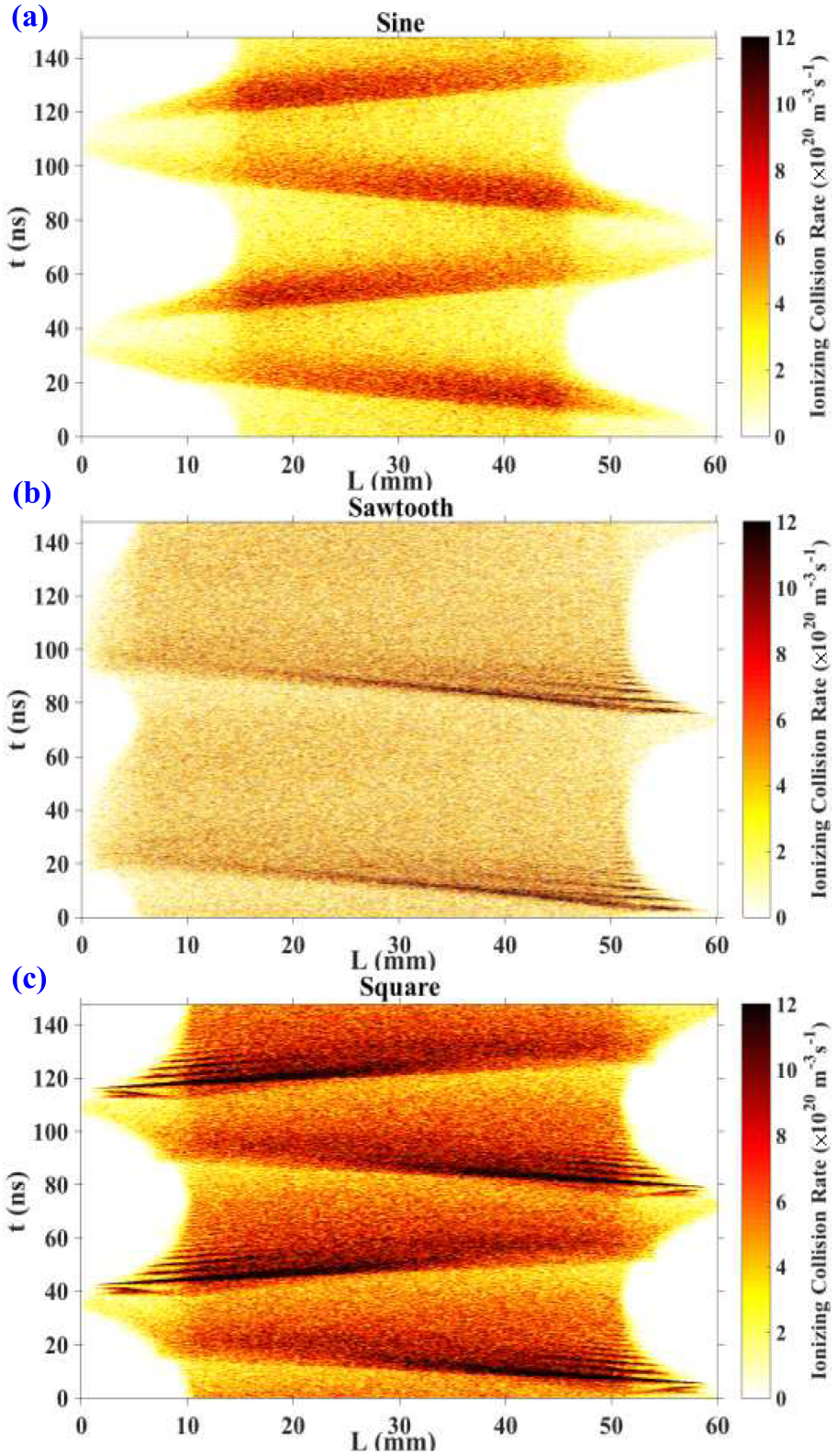

Figure 4. Spatio-temporal evolution of ionizing collision rates at different current waveforms; i.e. (a) sinusoidal (b) sawtooth and (c) square for 13.56 MHz for current densities of 50 A m^{-2}.

in figure 4(b) that multiple beam-like structures are present near to the grounded electrode during the sheath expansion. Similarly, in figure 4(c), intense multiple beam-like structures are created both near to the grounded and powered electrode during the time of sheath expansion. However, such multiple beam-like structures are absent in the case of the sinusoidal waveform. The reason for the creation of these multiple beam structures during the sheath expansion is due to

the high-frequency modulation on the instantaneous sheath edge position, which is similar to the sheath modulation in CCP discharges excited by multiple frequencies [26, 28, 71]. We will support this argument by investigating the non-linearity in the spatio-temporal profile of the electric field and higher harmonics generation on the instantaneous sheath edge position.

Figures 5(a)–(c) show the spatio-temporal evolution of the electric field for the sinusoidal, sawtooth, and square waveforms, respectively. The data shown here are for two RF periods, averaged over the last 100 RF cycles when the simulation results achieved a steady state condition. As shown in figure 5(a), for the sinusoidal case, the electric field is mostly confined in the sheath region and the bulk plasma is almost quasi-neutral. The instantaneous sheath edge position is smooth in this case. When the applied current waveform is changed to a sawtooth (see figure 5(b)) waveform, the temporal electric field at the sheath boundary near to the grounded electrode is substantially modified; i.e. high-frequency oscillations are observed on the instantaneous sheath edge position. The electric field here is also confined inside the sheath region and the bulk plasma is almost quasi-neutral. Furthermore, when the applied current waveform is square (see figure 5(c)), the temporal electric field at both the sheath edges, i.e. near to the grounded and powered electrode, is significantly modified and the high-frequency oscillations are clearly visible on the instantaneous sheath edge positions. These high-frequency modulations on the instantaneous sheath edge at both sheath edges is one of the principal factors responsible for driving the higher ionization rate and, as a result, producing higher plasma density in the system.

The presence of the electric field inside the bulk plasma is also significant here, which is termed 'electric field transients'. The formation of these electric field transients is reported in earlier articles [11, 14, 42, 72] and is mainly due to the higher sheath velocities that enhance energy gained by the electrons interacting with the oscillating sheath. Such electric field transients were mostly observed at higher driving frequencies [14, 61], whereas here they are present at a fundamental frequency of 13.56 MHz, but only in the case of the square waveform. We believe this is mostly related to the sheath velocity and higher harmonics on the instantaneous sheath position, which is higher in the case of the square waveform and is discussed in the following paragraph.

Figures 6(a) and (b) show the instantaneous sheath position and its fast Fourier transform (FFT), respectively, for different applied current waveforms. The graph in figure 6(a) is plotted for one RF period near to the grounded electrode. Again, the sheath width is calculated by observing the maximum position of the electron sheath edge from the electrode and where the quasi-neutrality breaks down. As shown in figure 6(a), for the sinusoidal waveform, the sheath width is expanding up to a maximum position of ∼15 mm from the grounded electrode. The instantaneous sheath position in this case is varying smoothly within the RF period; i.e. it is reaching up to the maximum position and collapsing back towards the grounded electrode.

In contrast to the sinusoidal waveform, the maximum sheath edge position is lower (∼9.5–9.7 mm) in the case of the sawtooth and square waveforms. Furthermore, both the sawtooth and square waveforms show high-frequency modulation on the instantaneous sheath position. These high-frequency oscillations are similar to the multi-frequency excited CCP discharges [26, 71]. Due to this, the conjugate sheath velocity modifies drastically and remains higher for the square waveform (7.35×10^5 m s^{-1}) as the number of oscillations on the instantaneous sheath edge position is higher in this case. The corresponding FFT is shown in figure 6(b). It is clear from figure 6(b) that the contribution of the fundamental frequency is highest in the case of the sinusoidal waveform and the higher harmonics contribution drops monotonically, whereas higher harmonic contents up to the seventh harmonics are clearly visible for the sawtooth and square waveforms (figure 6(b)). While comparing different waveforms, it is observed that the higher harmonic content (above the third harmonics) is maximum in the case of the square waveform. Thus, the presence of higher harmonic contents justifies production of higher plasma density in the case of the square waveform, as they are efficient in the power deposition. It is noteworthy that, due to asymmetry, the sawtooth waveform reflects high-frequency oscillations during the initial phase of the collapsing sheath edge (0.5–0.8 on the Y-axis in the RF period) and then smoothes out towards the grounded electrode.

The presence of higher harmonics on the instantaneous sheath edge position and therefore the higher sheath velocity drives the higher electron energy beams from near to the sheath edge. As discussed earlier, the sheath velocity is lowest for the sinusoidal waveform (2.2×10^5 m s^{-1}) and highest for the square waveform (7.35×10^5 m s^{-1}). These high-energy electrons create the electric field transients (figure 5(c)) inside the bulk plasma, which increase the population of high-energy electrons through non-linear interaction. This effect could be verified by analyzing the electron energy distribution function (EEDF). Figure 7 shows the EEDF at the center of the discharge for the three different waveforms. As displayed in figure 7, due to the strong electric field transients, both the low-energy electrons and high-energy tail-end electrons are highest in the case of the square waveform. The shape of the EEDF for the square waveform reveals three electron temperatures; i.e. bulk electron temperature (∼6 eV), mid-energy range (∼6 eV–33 eV), and high-energy tail-end electrons (>33 eV). The sawtooth waveform produces higher population of the low-energy electrons in comparison to the sinusoidal waveform; however, its tail-end electron population is slightly lower than the sinusoidal waveform. This effect is attributed to the asymmetric discharge behavior in the case of the sawtooth waveform.

As shown in figures 5(a) and (b), the electric field profile shows that the sheath is nearly symmetrical on both the powered and grounded electrode for the sinusoidal waveform (sheath voltage ∼1380 V at the powered and grounded electrode), whereas, for the sawtooth waveform, the powered electrode sheath is smaller in comparison to the grounded electrode. Thus, although the sheath velocity near

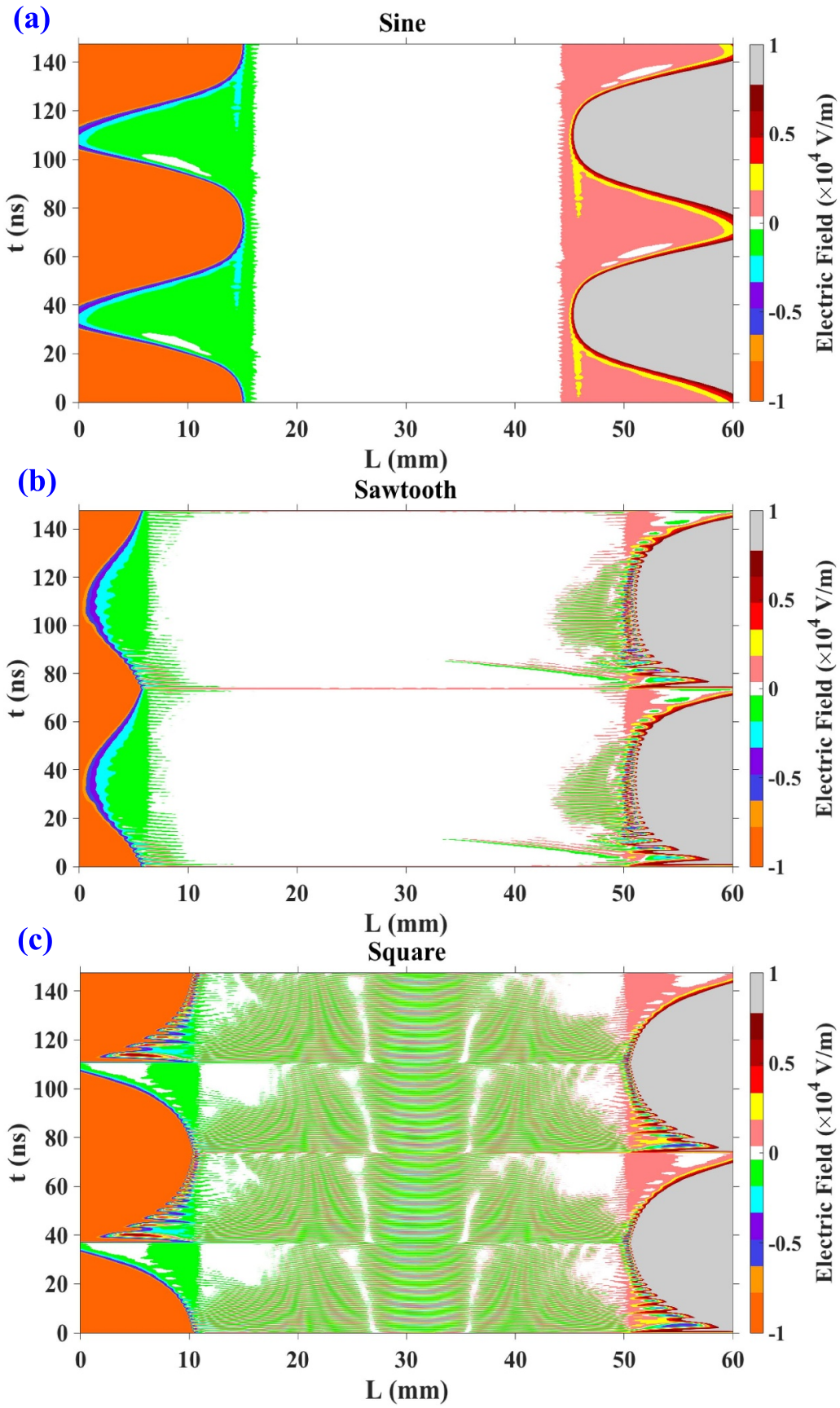

Figure 5. Spatio-temporal evolution of the electric field for two RF cycles at different applied current waveforms for 50 A m^{-2} and 13.56 MHz: (a) sinusoidal, (b) sawtooth, (c) square.

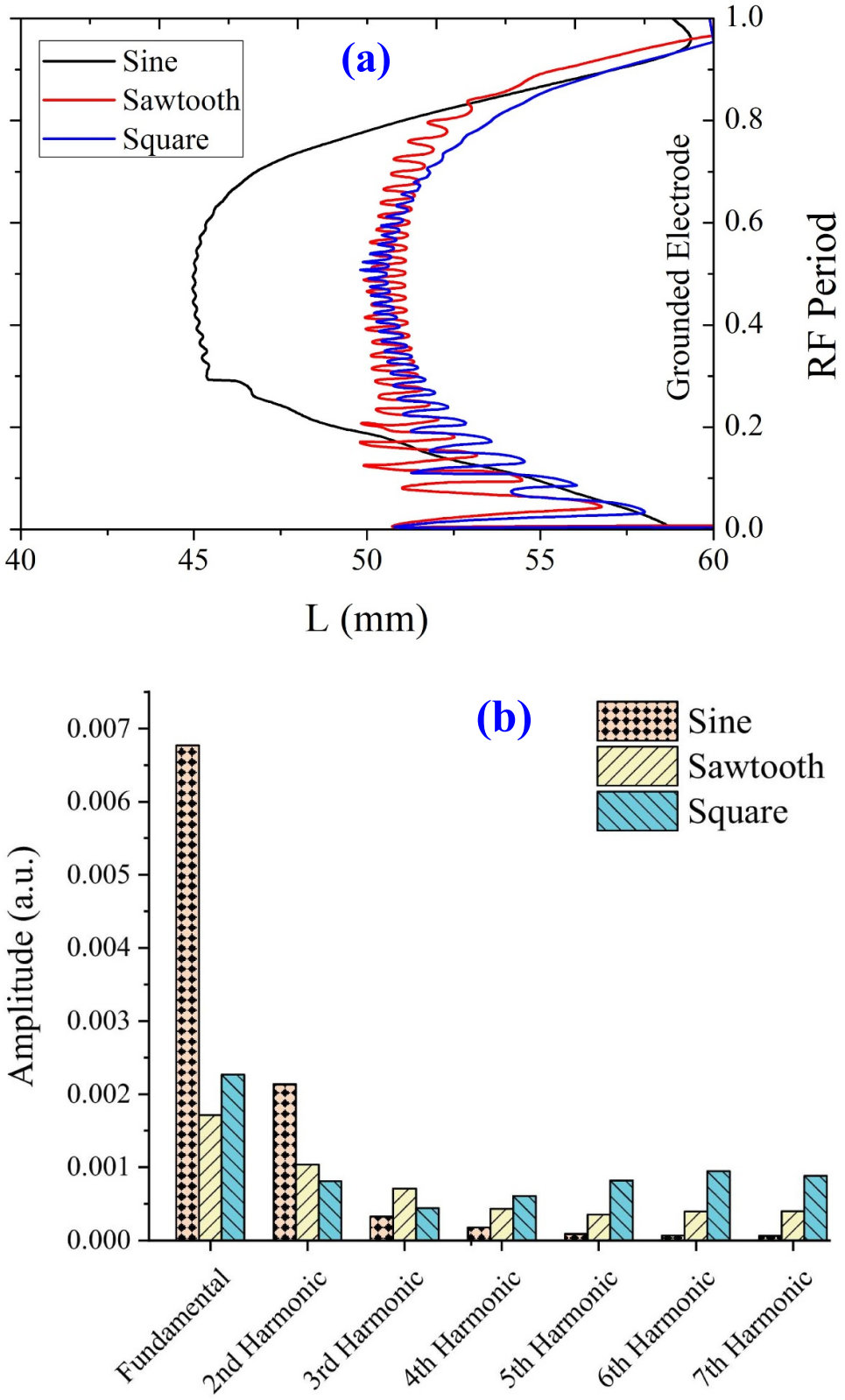

Figure 6. (a) Instantaneous sheath edge position for one RF period and (b) FFT of the instantaneous sheath edge for different applied current waveforms (sinusoidal, sawtooth, and square) for 13.56 MHz RF frequency and current densities of 50 A m^{-2}.

to the grounded electrode is higher for the sawtooth waveform and imparts higher energy to the electrons, they are not effectively confined on the opposite sheath edge as the powered electrode sheath voltage is lower (sheath voltage ∼350 V at the powered electrode and ∼560 V at the grounded electrode). Thus, the higher population of high-energy electrons for the sinusoidal waveform is due to the longer electron confinement, whereas, due to the asymmetric sheath, the sawtooth

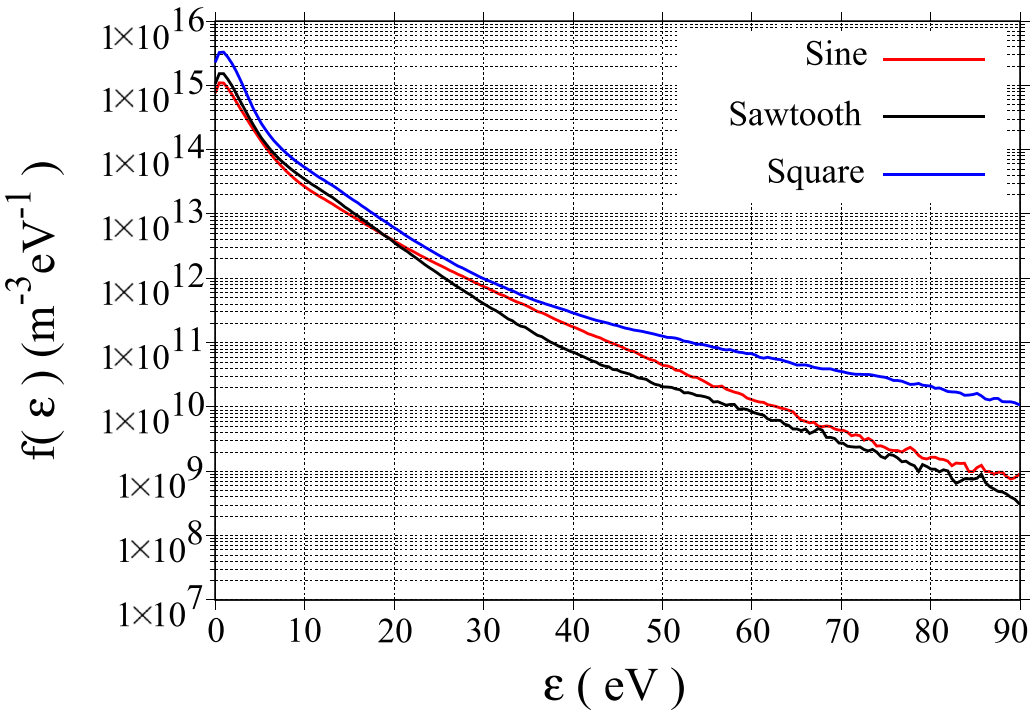

Figure 7. Electron energy distribution function at the center of the discharge for three different current waveforms. The current density amplitude is 50 A m^{-2} and the base frequency is 13.56 MHz.

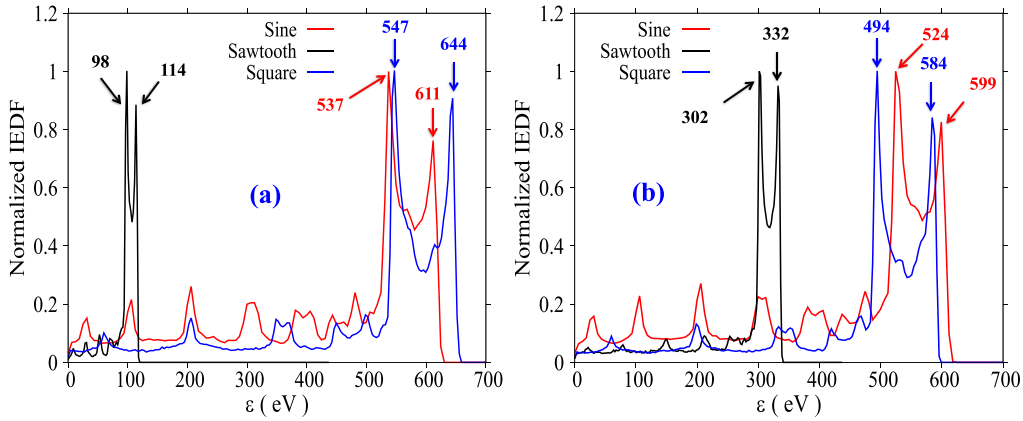

Figure 8. Ion energy distribution function (IEDF) for three different current waveforms at (a) the powered electrode and (b) the grounded electrode. The current density amplitude is 50 A m^{-2} and the RF frequency is 13.56 MHz.

waveform produces lower population of high-energy tail-end electrons (poor electron confinement).

On the other hand, the total (from ground state and excited states) time-averaged ionization rates (figure 3) are higher for the sawtooth waveform and therefore produce higher population of low-energy electrons. This effect is mainly attributed to the high-frequency oscillations on the instantaneous sheath edge position of the sawtooth waveform, which is not present in the case of the sinusoidal waveform.

Next, we study the effect of different current waveforms on the IEDF at the electrode surface. Figures 8(a) and (b) show the IEDF for the sinusoidal, sawtooth, and square waveform at the powered and grounded electrode, respectively. The simulation result predicts bimodal IEDF with multiple low-energy peaks for all the waveforms. The bimodal behavior is due to the collisionless ion transit through the RF sheath [30]. In the present case, the ratio of the sheath width (s) to ion means the free path (λ_i), s/λ_i, is ∼1–3.75 and therefore a bimodal energy distribution centered around the DC potential is observed. It is noteworthy that the asymmetry in the ion energy is highest in the case of the sawtooth waveform; i.e. the mean ion energy (the average of bimodal peak energies) is lower (∼106 eV) on the powered electrode when compared to the grounded electrode (∼317 eV). This asymmetry is attributed to the formation of DC self-bias and therefore the mean ion energy corresponds to the plasma potential (∼320 V) at the grounded electrode and plasma potential with respect to the DC self-bias (∼213 V) at the powered electrode. On the other hand, both the sinusoidal

and square waveforms produce nearly symmetrical and higher mean ion energies at both the powered and grounded electrode. This is attributed to the lower DC self-bias and higher values of the plasma potential, as shown in figure 2(b).

For the sinusoidal case, the mean ion energy is ∼570 eV, whereas, for the square, it is ∼539 eV at the grounded electrode and ∼596 eV at the powered electrode due to the negative self-bias of ∼52 V. As shown in figure 8, the energy separation (ΔE) of the bimodal peaks is lowest in the case of the sawtooth-like waveform (∼16 and ∼30 eV at the powered and grounded electrode, respectively) in comparison to the sine (∼75 eV at both the powered and grounded electrode) and square (∼97 and ∼90 eV at the powered and grounded electrode, respectively) waveforms. A drop in the sheath potential for the sawtooth waveform is one of the possible reasons for a decrease in the energy separation.

4. Summary and conclusion

In this work, we studied the effect of waveform tailoring on plasma density, ionization asymmetry, higher harmonics generation, theformation of electric field transients, and electron/ion energy distribution function. Two temporally asymmetric waveforms, sawtooth and square waveforms, were chosen and the results were compared with standard sinusoidal waveforms. The fundamental driving frequency was 13.56 MHz and the CCP discharge was operated by a current waveform at a constant current density amplitude of 50 A m^{-2} and 5 mTorr gas pressure. A large number ($N = 50$) of harmonics were chosen for creating an ideal sawtooth and square waveform.

The simulation results demonstrate that the square waveform produces the highest plasma density in comparison to sinusoidal and sawtooth waveforms. An enhanced plasma density in the case of the square waveform is due to the high-frequency oscillations (higher harmonics), up to 100 MHz, on the instantaneous sheath position that can penetrate the bulk plasma and therefore increase the total ionization rates from the ground state and excited states of the argon atom. The high-frequency oscillations are smaller in the case of the sawtooth waveform and, for the sinusoidal case, are negligible.

The maximum discharge asymmetry is observed in the case of the sawtooth-like waveform. An analysis of the time-averaged plasma potential shows a DC self-bias of ∼210 V for the sawtooth waveform, whereas for the square waveform it is −50 V, and no DC self-bias is observed in the case of the sinusoidal waveform. The corresponding sheath width for the sawtooth waveform is smaller near to the powered electrode (∼6 mm) in comparison to the grounded sheath (∼10.4 mm). For the square waveform, there is a slight difference (∼0.2 mm) between the sheath width at the powered and grounded electrode and for the sinusoidal waveform it is the same at both electrodes. The observed asymmetry is caused by the spatio-temporal ionization asymmetry, which shows that the ionization is higher near to the grounded sheath and lower near to the powered electrode sheath for the sawtooth waveform.

Both the sawtooth and square waveforms show multiple electric field transients. These multiple transients originate due to the high-frequency oscillations on the instantaneous sheath edge position. These high-frequency oscillations impart high energy to the electrons because of higher conjugate sheath velocities and thus the transients are stronger in the case of the square waveform penetrating the bulk plasma. For the sawtooth waveform, the energies of such transients are lower due to the lower number of high-frequency oscillations in comparison to the square waveform and therefore constraints near to the sheath region. Additionally, due to asymmetry, these transients are mostly observed near to the grounded sheath for the sawtooth waveform, whereas, for the square waveform, they originate from both the powered and grounded electrode sheaths.

For the square waveform, the EEDF represents three electron temperatures with a highly elevated electron tail when compared to the sinusoidal and sawtooth waveforms. The elevated electron tail is due to the penetration of multiple beam currents and better confinement of high-energy electrons between opposite sheaths. For the sawtooth waveform, the confinement of high-energy electrons is poor due to the asymmetric sheath; it therefore produces a lower population of high-energy electrons in comparison to the sinusoidal waveform. The shape of the IEDF is bimodal with multiple low-energy peaks for all the waveforms. The mean ion energies and energy separation of the bimodal peaks is lowest in the case of the sawtooth waveform because of the lower sheath voltage and higher in the case of the square and sinusoidal waveform. The mean ion energies of the bimodal peaks coincide with the plasma potential at the grounded electrode and plasma potential with respect to the DC self-bias on the powered electrode.

From the simulation results, it is concluded that the choice of waveform is critical for achieving maximum asymmetry and plasma density/ion flux simultaneously in CCP discharges using tailored waveforms.

Data availability statement

The data that support the findings of this study are available upon reasonable request from the authors.

Acknowledgments

Dr A Kuley is supported by the Board of Research in Nuclear Sciences (BRNS Sanctioned No. 39/14/05/2018-BRNS), the Science and Engineering Research Board EMEQ Program (SERB Sanctioned No. EEQ/2017/000164), the National Supercomputing Mission (NSM) (Ref. No.: DST/NSM/R&D_HPC_Applications/2021/04), and the Infosys Foundation Young Investigator Grant.

ORCID iDs

Sarveshwar Sharma https://orcid.org/0000-0002-0642-0247
Nishant Sirse https://orcid.org/0000-0002-7063-4100
Animesh Kuley https://orcid.org/0000-0003-2325-6597
Miles M Turner https://orcid.org/0000-0001-9713-6198

References

[1] Lieberman M and Lichtenberg A J 2005 *Principles of Plasma Discharges and Materials Processing* (New York: Wiley)
[2] Chabert P and Braithwaite N 2011 *Physics of Radio Frequency Plasmas* (Cambridge: Cambridge University Press)
[3] Popov O A and Godyak V A 1985 Power dissipated in low-pressure radio-frequency discharge plasmas *J. Appl. Phys.* **57** 53
[4] Vahedi V, Birdsall C K, Lieberman M A, DiPeso G and Rognlien T D 1993 Verification of frequency scaling laws for capacitive radio-frequency discharges using two-dimensional simulations *Phys. Fluids* B **5** 2719
[5] Bera K, Hoffman D, Shannon S, Delgadino G and Ye Y 2005 Frequency optimization for capacitively coupled plasma source *IEEE Trans. Plasma Sci.* **33** 382
[6] Colgan M J, Meyyappan M and Murnick D E 1994 Very high-frequency capacitively coupled argon discharges *Plasma Sources Sci. Technol.* **3** 181–9
[7] Wilczek S, Trieschmann J, Schulze J, Schuengel E, Brinkmann R P, Derzsi A, Korolov I, Donkó Z and Mussenbrock T 2016 The effect of the driving frequency on the confinement of beam electrons and plasma density in low-pressure capacitive discharges *Phys. Plasmas* **23** 063514
[8] Diomede P, Capitelli M and Longo S 2005 Effect of discharge voltage on capacitively coupled, parallel plate rf hydrogen plasmas *Plasma Sources Sci. Technol.* **14** 459–66
[9] Wilczek S, Trieschmann J, Schulze J, Schuengel E, Brinkmann R P, Derzsi A, Korolov I, Donkó Z and Mussenbrock T 2015 The effect of the driving frequency on the confinement of beam electrons and plasma density in low-pressure capacitive discharges *Plasma Sources Sci. Technol.* **24** 024002
[10] Sharma S, Sirse N, Kuley A, Sen A and Turner M M 2021 Driving frequency effect on discharge parameters and higher harmonic generation in capacitive discharges at constant power densities *J. Phys. D: Appl. Phys.* **54** 055205
[11] Sharma S, Sirse N, Sen A, Wu J S and Turner M M 2019 Electric field filamentation and higher harmonic generation in very high frequency capacitive discharges *J. Phys. D: Appl. Phys.* **52** 365201
[12] Sharma S, Abhijit S, Sirse N, Turner M M and Ellingboe A R 2018 Plasma density and ion energy control via driving frequency and applied voltage in a collisionless capacitively coupled plasma discharge *Phys. Plasmas* **25** 080705
[13] Sharma S, Sirse N, Turner M M and Ellingboe A R 2018 Influence of excitation frequency on the metastable atoms and electron energy distribution function in a capacitively coupled argon discharge *Phys. Plasmas* **25** 063501
[14] Sharma S, Sirse N, Kaw P K, Turner M M and Ellingboe A R 2016 Effect of driving frequency on the electron energy distribution function and electronsheath interaction in a low pressure capacitively coupled plasma *Phys. Plasmas* **23** 110701
[15] Abdel-Fattah E and Sugai H 2003 Electron heating mode transition observed in a very high frequency capacitive discharge *Appl. Phys. Lett.* **83** 1533
[16] Abdel-Fattah E, Bazavan M and Sugai H 2012 Electron energy distribution functions measured by Langmuir probe with optical emission spectroscopy in very high frequency capacitive discharge in nitrogen *Phys. Plasmas* **19** 113503
[17] Goto H H, Lowe H D and Ohmi T 1992 Dual excitation reactive ion etcher for low energy plasma processing *J. Vac. Sci. Technol.* A **10** 3048
[18] Goto H H, Lowe H D and Ohmi T 1993 Independent control of ion density and ion bombardment energy in a dual RF excitation plasma *IEEE Trans. Semicond. Manuf.* **6** 58
[19] Rauf S and Kushner M J 1999 Nonlinear dynamics of radio frequency plasma processing reactors powered by multifrequency sources *IEEE Trans. Plasma Sci.* **27** 1329
[20] Robiche J, Boyle P C, Turner M M and Ellingboe A R 2003 Analytical model of a dual frequency capacitive sheath *J. Phys. D: Appl. Phys.* **36** 1810
[21] Georgieva V and Bogaerts A 2005 Numerical simulation of dual frequency etching reactors: influence of external process parameterson the plasma characteristics *J. Appl. Phys.* **98** 023308
[22] Perret A, Chabert P, Jolly J and Booth J P 2005 Ion energy uniformity in high-frequency capacitive discharges *Appl. Phys. Lett.* **86** 021501
[23] Boyle P C, Ellingboe A R and Turner M M 2004 Independent control of ion current and ion impact energy onto electrodes in dual frequency plasma devices *J. Phys. D: Appl. Phys.* **37** 697
[24] Kim H C, Lee J K and Shon J W 2003 Analytic model for a dual frequency capacitive discharge *Phys. Plasmas* **10** 4545
[25] Sharma S 2013 Investigation of ion and electron kinetic phenomena in capacitively coupled radio-frequency plasma sheaths: a simulation study *PhD Thesis* Dublin City University (available at: http://doras.dcu.ie/17628/)
[26] Sharma S and Turner M M 2013 Critical evaluation of analytical models for stochastic heating in dual-frequency capacitive discharges *J. Phys. D: Appl. Phys.* **46** 285203
[27] Garrett C 2008 The dynamics of the charged particles in a dual frequency capacitively coupled dielectric etch reactor *PhD Thesis* Ecole Polytechnique, France
[28] Sharma S and Turner M M 2014 Investigation of wave emission phenomena in dual-frequency capacitive discharges using particle-in-cell simulation *J. Phys. D: Appl. Phys.* **47** 285201
[29] Kitajima T, Takeo Y, Petrovi´c Z L and Makabe T 2000 Functional separation of biasing and sustaining voltages in two-frequency capacitively coupled plasma *Appl. Phys. Lett.* **77** 489
[30] Lee J K, Manuilenko O V, Babaeva N Y, Kim H C and Shon J W 2005 Ion energy distribution control in single and dual frequency capacitive plasma sources *Plasma Sources Sci. Technol.* **14** 89
[31] Patterson M M, Chu H-Y and Wendt A E 2007 Arbitrary substrate voltage wave forms for manipulating energy distribution of bombarding ions during plasma processing *Plasma Sources Sci. Technol.* **16** 257
[32] Heil B G, Schulze J, Mussenbrock T, Brinkmann R P and Czarnetzki U 2008 Numerical modeling of electron beams accelerated by the radio frequency boundary sheath *IEEE Trans. Plasma Sci.* **36** 1404
[33] Heil B G, Czarnetzki U, Brinkmann R P and Mussenbrock T 2008 On the possibility of making a geometrically symmetric RF-CCP discharge electrically asymmetric *J. Phys. D: Appl. Phys.* **41** 165202
[34] Donkó Z, Schulze J, Heil B G and Czarnetzki U 2009 PIC simulations of the separate control of ion flux and energy in

CCRF discharges via the electrical asymmetry effect *J. Phys. D: Appl. Phys.* **42** 025205
[35] Korolov I, Donkó Z, Czarnetzki U and Schulze J 2012 The effect of the driving frequencies on the electrical asymmetry of dual-frequency capacitively coupled plasmas *J. Phys. D: Appl. Phys.* **45** 465205
[36] Bora B, Bhuyan H, Favre M, Wyndham E and Wong C S 2013 Dual radio frequency plasma source: understanding via electrical asymmetry effect *J. Appl. Phys.* **113** 153301
[37] Lafleur T and Booth J P 2013 Frequency dependence of the electrical asymmetry effect in dual-frequency capacitively coupled discharges *Appl. Phys. Lett.* **102** 154104
[38] Bruneau B, Novikova T, Lafleur T, Booth J P and Johnson E V 2014 Ion flux asymmetry in radiofrequency capacitively-coupled plasmas excited by sawtooth-like waveforms *Plasma Sources Sci. Technol.* **23** 065010
[39] Bruneau B, Novikova T, Lafleur T, Booth J P and Johnson E V 2015 Control and optimization of the slope asymmetry effect in tailored voltage waveforms for capacitively coupled plasmas *Plasma Sources Sci. Technol.* **24** 015021
[40] Bruneau B, Gans T, O'Connell D, Greb A, Johnson E V and Booth J P 2015 Strong ionization asymmetry in a geometrically symmetric radio frequency capacitively coupled plasma induced by sawtooth voltage waveforms *Phys. Rev. Lett.* **114** 125002
[41] Lafleur T, Boswell R W and Booth J P 2012 Enhanced sheath heating in capacitively coupled discharges due to non-sinusoidal voltage waveforms *Appl. Phys. Lett.* **100** 194101
[42] Sharma S, Sirse N and Turner M M 2020 High frequency sheath modulation and higher harmonic generation in a low pressure very high frequency capacitively coupled plasma excited by sawtooth waveform *Plasma Sources Sci. Technol.* **29** 114001
[43] Wang S-B and Wendt A E 2000 Control of ion energy distribution at substrates during plasma processing *J. Appl. Phys.* **88** 643
[44] Schulze J, Schüngel E, Czarnetzki U and Donkó Z 2009 Optimization of the electrical asymmetry effect in dual-frequency capacitively coupled radio frequency discharges: experiment, simulation, and model *J. Appl. Phys.* **106** 063307
[45] Sharma S, Mishra S K, Kaw P K, Das A, Sirse N and Turner M M 2015 Collisionless sheath heating in current-driven capacitively coupled plasma discharges via higher order sinusoidal signals *Plasma Sources Sci. Technol.* **24** 025037
[46] Baloniak T, Reuter R and von Keudell A 2010 Fundamental aspects of substrate biasing: ion velocity distributions and nonlinear effects *J. Phys. D: Appl. Phys.* **43** 335201
[47] Lafleur T and Booth J P 2012 Control of the ion flux and ion energy in CCP discharges using non-sinusoidal voltage waveforms *J. Phys. D: Appl. Phys.* **45** 395203
[48] Delattre P A, Lafleur T, Johnson E V and Booth J P 2013 Radio-frequency capacitively coupled plasmas excited by tailored voltage waveforms: comparison of experiment and particle-in-cell simulations *J. Phys. D: Appl. Phys.* **46** 235201
[49] Lafleur T, Delattre P A, Johnson E V and Booth J P 2012 Separate control of the ion flux and ion energy in capacitively coupled radio-frequency discharges using voltage waveform tailoring *Appl. Phys. Lett.* **101** 124104
[50] Lafleur T, Delattre P A, Johnson E V and Booth J P 2013 Capacitively coupled radio-frequency plasmas excited by tailored voltage waveforms *Plasma Phys. Control. Fusion* **55** 124002
[51] Hrunski D *et al* 2013 Deposition of microcrystalline intrinsic silicon by the electrical asymmetry effect technique *Vacuum* **87** 114
[52] Schuengel E, Hofmann R, Mohr S, Schulze J, Ropcke J and Czarnetzki U 2015 Evaluation of the electrical asymmetry effect by spectroscopic measurements of capacitively coupled discharges and silicon thin film depositions *Thin Solid Films* **574** 60
[53] Fischer G, Drahi E, Lebreton F, Bulkin P, Poulain G and Johnson E V 2017 Nanotextured silicon surfaces using tailored voltage waveform plasmas: impact of ion bombardment energy on etching dynamics and passivation *33rd European Photovoltaic Solar Energy Conf. and Exhibition (Amsterdam)* (https://doi.org/10.4229/EUPVSEC20172017-2AV.2.33)
[54] Wang J K and Johnson E V 2017 Electrode-selective deposition/etching processes using an SiF_4/H_2/Ar plasma chemistry excited by sawtooth tailored voltage waveforms *Plasma Sources Sci. Technol.* **26** 01LT01
[55] Z Donkó, A Derzsi, M Vass, J Schulze, Schuengel E and Hamaguchi S 2018 Ion energy and angular distributions in lowpressure capacitive oxygen RF discharges driven by tailored voltage waveforms *Plasma Sources Sci. Technol.* **27** 104008
[56] Turner M M, Hutchinson A W, Doyle R A and Hopkins M B 1996 Heating mode transition induced by a magnetic field in a capacitive rf discharge *Phys. Rev. Lett.* **76** 2069
[57] Boyle P C, Ellingboe A R and Turner M M 2004 Electrostatic modelling of dual frequency rf plasma discharges *Plasma Sources Sci. Technol.* **13** 493
[58] Lauro-Taroni L, Turner M M and Braithwaite N S J 2004 Analysis of the excited argon atoms in the GEC RF reference cell by means of one-dimensional PIC simulations *J. Phys. D: Appl. Phys.* **37** 2216
[59] Turner M M 2013 Numerical effects on energy distribution functions in particle-in-cell simulations with monte carlo collisions: choosing numerical parameters *Plasma Sources Sci. Technol.* **22** 055001
[60] Conway J, Kechkar S, O Connor N, Gaman C, Turner M M and Daniels S 2013 Use of particle-in-cell simulations to improve the actinometry technique for determination of absolute atomic oxygen density *Plasma Sources Sci. Technol.* **22** 045004
[61] Sharma S, Sirse N, Sen A, Turner M M and Ellingboe A R 2019 Influence of select discharge parameters on electric field transients triggered in collisionless very high frequency capacitive discharges *Phys. Plasmas* **26** 103508
[62] Sharma S, Sirse N, Kuley A and Turner M M 2020 Electric field nonlinearity in very high frequency capacitive discharges at constant electron plasma frequency *Plasma Sources Sci. Technol.* **29** 045003
[63] Hockney R W and Eastwood J W 1988 *Computer Simulation Using Particles* (Bristol: Adam Hilger)
[64] Birdsall C K 1991 *Plasma Physics via Computer Simulation* (Bristol: Adam Hilger)
[65] Turner M M, Derzsi A, Donko Z, Eremin D, Kelly S J, Lafleur T and Mussenbrock T 2013 Simulation benchmarks for low-pressure plasmas: capacitive discharges *Phys. Plasmas* **20** 013507
[66] Shahid R and Kushner Mark J 1997 Argon metastable densities in radio frequency Ar, Ar/O_2 and Ar/CF4 electrical discharges *J. Appl. Phys.* **82** 2805
[67] Sternglass E J 1957 Theory of secondary electron emission by high-speed ions *Phys. Rev.* **108** 1
[68] Horvath B, Schulze J, Donko Z and Derzsi A 2018 The effect of electron induced secondary electrons on the

characteristics of low-pressure capacitively coupled radio frequency plasmas *J. Phys. D: Appl. Phys.* **51** 355204
[69] Turner M M and Chabert P 2014 A radio-frequency sheath model for complex waveforms *Appl. Phys. Lett.* **104** 164102
[70] Turner M M and Chabert P 2017 A model for tailored-waveform radiofrequency sheaths *J. Phys. D: Appl. Phys.* **50** 23LT02
[71] Sharma S, Mishra S K, Kaw P K and Turner M M 2017 The effect of intermediate frequency on sheath dynamics in collisionless current driven triple frequency capacitive plasmas *Phys. Plasmas* **24** 013509
[72] Sharma S, Sirse N, Kuley A and Turner M M 2021 Ion energy distribution function in a very high frequency capacitive discharges excited by sawtooth waveform *Phys. Plasmas* **28** 103502